

Near theoretical microwave loss in hot isostatic pressed (hipped) polycrystalline yttrium iron garnet

Alexey V. Nazarov,^{a)} David Ménard,^{b)} Jerome J. Green, and Carl E. Patton
Department of Physics, Colorado State University, Fort Collins, Colorado 80523

Gil M. Argentina
Pacific Ceramics, Inc., 824 San Aleso Avenue, Sunnyvale, California 94085

H. J. Van Hook
Consultant, 89 Meriam Street, Lexington, Massachusetts 02420

(Received 5 May 2003; accepted 10 September 2003)

The ferromagnetic resonance (FMR) linewidth, the field dependent effective linewidth, and the parallel pump spin wave linewidth were measured for spheres and disks prepared from a block of hot isostatic pressed (hipped) polycrystalline yttrium iron garnet (YIG). All linewidths as well as static magnetization data indicate close to 100% density. Vibrating sample magnetometer measurements give an average saturation induction $4\pi M_s$ of 1825 G. The FMR half-power linewidths for the spheres at 9.5 GHz were 13 Oe. Linewidths measured over the 9.5–18 GHz frequency range show a small but distinct drop and agree with Schlömann's theory of anisotropy-dominated two-magnon scattering for polycrystalline ferrites. The effective linewidth versus field data at 10 GHz show a region of strong absorption that corresponds to the width of the spin wave manifold for low wave numbers and a high field value of about 2 Oe. Parallel pumping measurements give minimum spin wave linewidths of 1.2 and 0.6 Oe at 9 and 16.7 GHz, respectively. The 16.7 GHz spin wave linewidths correspond to half-frequency spin waves at 8.35 GHz. The extrapolated linewidths at zero wave number are about 0.5 Oe and match the established intrinsic linewidths expected for YIG single crystals at 8–9 GHz. The spin wave linewidths increase linearly with wave number and are consistent with a transit time scattering process with scattering lengths that are about ten times greater than the average grain size. © 2003 American Institute of Physics. [DOI: 10.1063/1.1622996]

I. INTRODUCTION

The ferromagnetic resonance (FMR) losses in polycrystalline ferrites are generally associated with the microstructure of the material. For typical coarse-grain sintered ferrites with a small porosity and a low magnetocrystalline anisotropy, the dominant loss mechanism is two-magnon scattering. The two sources of the scattering are (1) the anisotropy of the randomly oriented crystalline grains and (2) pores, grain boundaries, and residual second phase components. Even after four decades of work in this field, a thorough understanding of these losses remains elusive. The anisotropy and porosity mechanisms were first treated theoretically by Schlömann.^{1,2} Sparks and co-workers have also provided detailed analyses of porosity and pit scattering processes.^{3,4} The anisotropy and porosity processes have been verified through FMR linewidth and effective linewidth measurements.^{5–8} These references also show that it is extremely difficult to isolate the anisotropy scattering process because of the residual porosity.⁹ In polycrystalline yttrium iron garnet (YIG), for example, the porosity contribution to

the FMR linewidth at 10 GHz is approximately 23 Oe per percent porosity.⁵ Porosities as small as a few tenths percent can make a significant contribution to the linewidth.

From the above, it is clear that one can obtain the lowest possible linewidth in a given polycrystalline ferrite only if the material is extremely dense and anisotropy scattering processes are dominant. There are two established ceramic processes which may be used to achieve a high ferrite density, namely, hot pressing¹⁰ and hot isostatic pressing (hipping).^{11,12} This work reports on FMR linewidth and other microwave measurements on ultradense polycrystalline YIG materials which were produced by the hipping process. The measured densities were very close to theoretical densities. The measured linewidths closely match computed linewidths from the anisotropy-dominated two-magnon scattering theory of Schlömann.² These data represent experimental linewidth results on polycrystalline ferrite materials corresponding to pure anisotropy scattering. The high-field effective linewidth and spin wave linewidths are much smaller than the FMR linewidths and are consistent with previous work on microwave loss and microstructure.

Section II describes the materials and the preparation techniques, and discusses static magnetic properties. Section III gives a brief overview of the microwave loss problem, identifies the key linewidth parameters of interest, namely, the FMR linewidth, the effective linewidth, and the spin wave linewidth, and summarizes the various linewidth mea-

^{a)}Author to whom correspondence should be addressed; present address: Seagate Recording Heads, 7801 Computer Avenue South, Bloomington, MN 55435; electronic mail: Alexey.V.Nazarov@seagate.com

^{b)}Present address: Département de Génie Physique, Ecole Polytechnique de Montréal, C.P. 6079, Succ. Centre-Ville, Montréal (Québec), Canada H3C 3A7.

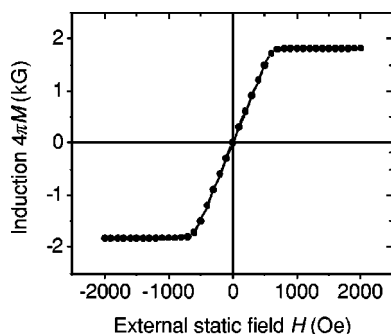


FIG. 1. Magnetic induction $4\pi M$ versus the external static field H for the hipped yttrium iron garnet 2.04 mm diam sphere sample. The solid points show the data and the lines connect the points.

surement techniques. The FMR linewidth data and analysis, as well as effective linewidth results, are given in Sec. IV. Section V presents the high-power spin wave instability parallel pumping data and a spin wave linewidth analysis based on these data. Section VI gives a summary and conclusion.

II. MATERIALS AND STATIC MAGNETIC PROPERTIES

The starting material was a conventionally sintered polycrystalline YIG material from Pacific Ceramics, Inc. This material was prepared from starting yttrium oxide powders with a rare earth impurity content below 0.01%. The residual porosity was less than 1% and the half-power FMR linewidth was about 27 Oe at 10 GHz.

Small blocks of these materials were then subjected to a hipping process in an argon atmosphere. The starting argon pressure in the chamber was 470 bar. The temperature and pressure were gradually increased to 1400 °C and 1000 bar, respectively, over 10 h and then held at this soak point for 3 h. The system was then cooled and vented back to room temperature and pressure over about 20 h. The measured density of the hipped YIG material was 5.172 g/cm³. This matches the theoretical YIG density. The average grain size was 8 μm. Disks and spheres in the millimeter size range were fabricated from the interior regions of the hipped blocks in order to avoid possible problems with oxygen-deficient surface regions. The nearly complete elimination of porosity for these hipped samples was confirmed from static magnetization and FMR linewidth measurements. Representative results are given below. The specific data shown are for a 2.04 mm diam sphere and a 3.0 mm diam, 0.46 mm thick disk.

A commercial vibrating sample magnetometer system was used for magnetic moment versus field measurements. Calibrated curves of the magnetic induction $4\pi M$ as a function of the static external field H and values of the saturation induction $4\pi M_s$ were obtained from these data, the sample mass, and the measured density noted above. The experimental error in the $4\pi M$ values was about ± 20 G.

Figure 1 shows a representative hysteresis loop of $4\pi M$ versus H for the 2.04 mm diam sphere sample. The loop has the expected appearance for a dense polycrystalline ferrite with a linear low-field response and very little hysteresis, a distinct break at the saturation field, and a flat response at higher field. The data give a saturation induction $4\pi M_s$ value of 1.825 kG. The fitted slope of the linear low field response is 2.99 kG/kOe. There was a very small amount of hysteresis. Further measurements on an expanded field scale gave a coercive force of 0.2 Oe.

The hysteresis data in Fig. 1 match those expected for dense polycrystalline YIG. The saturation induction is in the same range as reported literature values for single crystals. The $4\pi M_s$ value of 1825 G is somewhat high but within experimental error, relative to published values.¹³ The slope of the low field matches the demagnetizing response of 3 kG/kOe expected for spherical samples. The microwave linewidth data provide a more sensitive measure of the sample density. These data are discussed in detail in the next section.

Table I gives a summary of the results from the static measurements, along with a listing of the 9.5 GHz FMR fields and linewidths for the sphere and the disk. The disk was measured with the static field in plane or normal to the disk plane, as indicated. The table lists the saturation induction $4\pi M_s$ and the saturation field H_s obtained for these three sample geometries. The saturation field H_s also corresponds to the maximum demagnetizing field for the sample. The linewidth and threshold field results are discussed in Secs. IV and V.

The static data in Table I support the conclusions obtained from Fig. 1. The sphere and disk data show consistent values of $4\pi M_s$. The matching up of these data within experimental error is noteworthy, since the samples were cut from different regions of the hipped block. The measured saturation fields are consistent with the $4\pi M_s$ determinations and the different shapes and field directions. The H_s for the sphere is within a few oersteds of the expected value of $4\pi M_s/3$. From the estimated error of ± 20 G for the $4\pi M_s$ determinations, one can place only an upper bound of 1% on the porosity of the hipped materials. The microwave data

TABLE I. Selected data for the hipped yttrium iron garnet sphere and disk samples. The columns show the sample and field direction, the saturation induction $4\pi M_s$, the saturation field H_s , the ferromagnetic resonance (FMR) field H_0 at 9.5 GHz, and the half-power FMR linewidth ΔH_0 at 9.5 GHz.

Sample (field direction)	Saturation induction $4\pi M_s$ (G)	Saturation field H_s (Oe)	FMR field H_0 at 9.5 GHz (kOe)	FMR linewidth ΔH_0 at 9.5 GHz (Oe)
Sphere	1825	610	3.47	13
Disk (in plane)	1825	170	2.89	22
Disk (normal to plane)	1820	1480	4.64	14

will show that the actual porosity is much lower, and has an upper bound of about 0.02%.

III. MICROWAVE LINEWIDTH PARAMETERS AND MEASUREMENT OVERVIEW

The microwave relaxation processes in magnetic materials are generally described by three linewidth parameters, the FMR linewidth, the field-dependent effective linewidth, and the spin wave linewidth. The FMR linewidth ΔH_0 corresponds to the width in field at half maximum of the resonance power absorption profile. The effective linewidth describes the off-resonance loss and corresponds to the relaxation of the uniform precession for fields away from the resonance peak. The spin wave linewidth is a measure of the actual relaxation rate of parametric spin waves generated through nonlinear processes. In general, this linewidth depends on the wave number and the direction of propagation for the relevant spin waves. In high-quality single crystals, the spin wave linewidth for low wave numbers is the same as the FMR linewidth for modes at the same frequency. If the single crystal specimen has macroscopic defects such as cracks or a rough surface, for example, the FMR linewidth may increase while the spin wave linewidth remains the same.³ Up to now, the effective linewidth has not been measured in single crystals due to the measurement difficulties caused by high order magnetostatic modes and the very low loss away from resonance.

Linewidths in polycrystals are generally much larger than in single crystals. In polycrystalline materials, the three types of linewidths are generally associated with different relaxation mechanisms. The FMR linewidth, for example, is affected by inhomogeneities and two-magnon scattering processes. In polycrystals, this linewidth can be quite large. The increase is generally attributed to some aspects of the microstructure, such as porosity, grain size, grain size distribution, or anisotropy in the randomly oriented crystallites.^{9,14} On the other hand, the off-resonance effective linewidth, especially at high field, is not affected by two-magnon scattering and can be much smaller. The spin wave linewidth represents the relaxation rate of the renormalized spin wave modes that exhibit a threshold loss effect under parametric excitation. This linewidth can be extremely small. The measurement of all three types can give a much clearer picture of the applicable loss mechanisms than any single linewidth alone.

Ferromagnetic resonance linewidths were measured from 9.5 to 18 GHz. Standard shorted waveguide techniques were used.¹⁵ For each measurement frequency, the sample was carefully positioned in the center of the waveguide one-half wavelength from the shorted end. The half-power FMR linewidth ΔH_0 was then obtained as the difference between the values of the static field for which the negative imaginary part of the susceptibility is equal to one-half its maximum value. The measured linewidths were accurate to about ± 0.2 Oe.

The effective linewidth was determined as a function of field for a single excitation frequency of 10 GHz. For these measurements, the sample was placed in the center of a high- Q TE₀₁₁ cylindrical transmission cavity. The cavity Q factor and the resonance frequency f_c were measured as a function

of the applied field based on procedures similar to those given in Ref. 16. From these Q and f_c versus field data, the complex susceptibility and the corresponding effective linewidth ΔH_{eff} were obtained. Due to the small change in the Q factor far from resonance, the error in the effective linewidth ΔH_{eff} measurements was ± 0.5 Oe. Complete details of the technique may be found in Ref. 9 and other references therein.

The spin wave linewidth ΔH_k does not correspond to an actual linewidth. Rather, ΔH_k simply expresses the relaxation rate of parametrically excited spin waves in linewidth units. One measures this relaxation rate and obtains the corresponding ΔH_k from the spin wave instability threshold fields h_{crit} . In general, the determination of the ΔH_k value at a given field is done in three steps. First, one makes a microwave threshold field measurement. Second, one performs a theoretical analysis to determine the particular spin wave pair out of all available spin waves at one-half the pump frequency that has the lowest threshold.¹⁷ Third, one equates the theoretical minimum threshold to the measured one and computes the spin wave linewidth. The spin wave linewidth analysis for the parallel pumping case in isotropic polycrystalline ferrite spheres will be given in Sec. V B.

A high-power microwave pulse spectrometer system was used to measure the spin wave instability threshold field h_{crit} as a function of the applied static field.^{18,19} The input microwave pulses were 50 μs wide and the nominal repetition rate was 40 Hz. Peak input powers were in the 1–2 kW range. Separate waveguide setups were used for measurements at 9 and 16.7 GHz. At 9.0 GHz, a high- Q TE₀₁₁ cylindrical cavity was used. At 16.7 GHz, a standard TE₁₀₂ rectangular cavity was used. The experimental h_{crit} results were obtained directly from the values of the incident power at the point where the trailing edge of the pulse showed a visible nonlinear response. The low-duty cycle pulse based h_{crit} determination technique eliminated problems with sample heating. For both frequencies, the measurements were made with the sample in the center of the cavity. The error in these measurements was about 5%. Spin wave linewidth values were then obtained from the h_{crit} data and the standard parallel pumping analysis of Schlömann *et al.*²⁰

IV. FERROMAGNETIC RESONANCE LINEWIDTH AND OFF-RESONANCE EFFECTIVE LINEWIDTH

A. Ferromagnetic resonance linewidth

The nominal 9.5 GHz FMR results for the sphere and the disk sample are summarized in Table I. The data show that the lowest linewidth of 13 Oe is obtained for the sphere. The normal to plane field configuration for the disk gives a linewidth which is about 1 Oe larger, while the linewidth for the in-plane configuration is almost double these values. The extremely low linewidth for the sphere is an important indicator of a near zero porosity for the hipped polycrystalline material. The increase in the linewidth for the in-plane magnetized disk is consistent with this indicator. These points will be considered shortly. The FMR field for the sphere is consistent with a Landé g factor for the hipped YIG of about 1.95, or slightly less than the free electron value of 2.

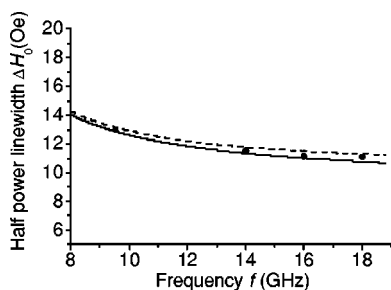


FIG. 2. Ferromagnetic resonance (FMR) half-power linewidth as a function of frequency f for the hipped yttrium iron garnet 2.04 mm diam sphere. The solid circles show the data. The solid line shows the calculated linewidth for the two-magnon anisotropy scattering (TMAS) process. The dashed line shows the TMAS response shifted upward by $0.03f$ to account for the intrinsic linewidth.

The linewidth data in Table I provide a clear indication that the losses are predominantly due to two-magnon scattering. The 13 Oe linewidth for the sphere is almost exactly what one would expect for a two-magnon process due to the magnetocrystalline anisotropy in the randomly oriented crystalline grains in the dense polycrystalline material.² The small value of the sphere linewidth and the match with anisotropy theory shows that the porosity is extremely small. Typically, porosity gives an additional two-magnon linewidth which is about 23 Oe per percent for YIG spheres.⁵ The matching places an upper limit on the porosity of about 0.02%. Further details of this process are given below. The large increase in the linewidth as one goes to the in-plane magnetized disk case also supports a two-magnon process. This is because the density of states for the scattering increases substantially for this configuration and gives a larger two-magnon linewidth.

Additional linewidth versus frequency measurements as described in Sec. II were made in order to check the applicability of the two-magnon anisotropy scattering process to the data. For a sphere shaped sample, there is a well defined change in the density of low-wave-number states as the FMR frequency is changed. This variation in the density of states can appear as a characteristic change in the linewidth with frequency. For samples in which the grains or other scattering centers are in the 1–10 μm size range, the scattering is confined to relatively low wave numbers k below about 10^3 rad/cm. The initial evidence for a two-magnon scattering FMR relaxation process in YIG single crystals came from direct observations of a peak in the linewidth at about 4 GHz for spheres with rough surfaces. This peak corresponds to the frequency at which the FMR frequency moves through the top of the spin wave band in the $k=0$ limit and for which the density of states goes through a maximum. As the frequency is increased above 4 GHz, the linewidth decreases as the density of states decreases. Details of this density of states effect may be found in Refs. 3 and 9 and the original sources cited therein.

Figure 2 shows the results of the sphere linewidth versus frequency measurements and the corresponding anisotropy scattering two-magnon analysis. The graph shows the half-power linewidth ΔH_0 as a function of frequency f from 8 to 19 GHz. Note the suppressed zero for the vertical linewidth

axis. The solid circles show the data. The solid line shows a computed two-magnon anisotropy scattering (TMAS) linewidth versus frequency response based on the theory of Schlömann in Ref. 2. The dashed line shows a slightly up-shifted theoretical curve based on the additional frequency-dependent linewidth contribution expected for single crystals. Both curves are considered in more detail below.

The match between the data and the theory will be considered shortly. The data alone, even without the theory, indicate that these materials are very close to theoretical density. This conclusion is based on two observations. First, the 11–13 Oe linewidths are all small. As noted above, even a small porosity would lead to a substantial linewidth increase in the range of 23 Oe per percent of porosity. Second, it is noteworthy that the linewidth is found to decrease slightly with increasing frequency. Porosity line broadening is known to produce a linewidth which *increases* with frequency.^{5,6} The decrease in linewidth with frequency as well as the 11–13 Oe values are connected with the change in the density of states and scattering solely due to anisotropy, *with no porosity effects*.

In Ref. 2, Schlömann outlined a basic theory for the FMR linewidth associated with two-magnon scattering from the grains in a polycrystalline ferrite due to the randomly oriented magnetocrystalline anisotropy in the individual grains. The theory was done in the so-called “coarse-grain” approximation for which the scattering is strong only for small spin wave wave numbers. The Schloemann theory gives a convenient closed form expression for the TMAS linewidth which may be written as

$$\Delta H_{\text{TMAS}} = 2.07(4H_A^2/4\pi M_s)G(\omega/|\gamma|4\pi M_s). \quad (1)$$

The H_A parameter denotes an effective anisotropy field K_1/M_s , where K_1 is the first order cubic anisotropy energy constant. For YIG, H_A is approximately -45 Oe.¹³ The G function is given by

$$G(x) = \frac{x^2 - x/3 + 19/360}{\sqrt{(x-1/3)^3(x-2/3)}}. \quad (2)$$

In the G function argument in Eq. (1), ω denotes the angular frequency and γ is the applicable gyromagnetic ratio for the ferrite. For YIG, $|\gamma|/2\pi$ is close to the free electron value of 2.8 MHz/Oe.

Apart from the numerical factors in Eq. (1), the form of the response may be easily understood from physical considerations. First, the basic inhomogeneous line broadening due to the variation in the anisotropy axes from grain to grain would give a linewidth proportional to H_A . One must then multiply this simple line broadening term by the ratio $H_A/4\pi M_s$ in order to account for dipole narrowing, that is, the tendency of the individual moments to precess together in phase in order to minimize the dipole-dipole energy of the system. Finally, the G function gives the frequency dependence of the density of the low- k spin wave states degenerate with the signal frequency ω . The function as given is valid only in the coarse-grain limit noted above, for which the

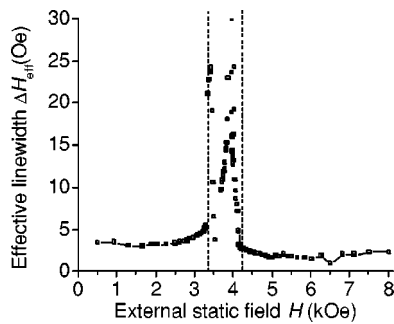


FIG. 3. Effective linewidth ΔH_{eff} as a function of the external static field H at 10 GHz for the hipped YIG 2.04 mm diam sphere. The vertical dashed lines indicate the upper and lower field boundaries of the spin wave manifold in the zero wave number limit. The data points inside the manifold region correspond to large degradations in the cavity Q and do not represent the true losses. Some of these data points are not shown due to the scale of the vertical axis.

scattering is limited to low- k modes. In this limit, $G(f)$ gives a slightly decreasing function of frequency as indicated by the lines in Fig. 2.

The solid line in Fig. 2 shows the computed TMAS linewidth as a function of the frequency f , based on the numerical parameters cited above and the sphere $4\pi M_s$ value from Sec. II and Table I. Note that the solid curve is obtained with no adjustable parameters. The dashed curve shows the TMAS result with an added upshift by $(0.03 \text{ Oe/GHz})f$ to account for the intrinsic linewidth which would still be present for a YIG crystal. The intrinsic linewidth varies linearly with frequency and is about 0.3 Oe at 9 GHz.³ One can see that the matching of the computed response, with or without the small intrinsic correction, with the data is extremely good. Keep in mind that the error in the measured linewidths is about ± 0.2 Oe. The matching, well within experimental error, provides further support for the presence of an extremely low porosity and a dominant TMAS linewidth process.

B. Off-resonance effective linewidth

Figure 3 shows the results of the sphere off-resonance effective linewidth ΔH_{eff} measurements as a function of the external static field H . The solid squares show the data. The vertical dashed lines indicate the field boundaries of the spin wave manifold at zero wave number. The lines connecting the data points outside the manifold region are intended as a guide to the eye only. The data show a flat response at fields below the low-field manifold edge and above the high-field manifold edge. The low-field level of about 3 Oe is somewhat larger than the high-field level of about 2 Oe. The data between 5 and 8 kOe give a ΔH_{eff} of 1.7 ± 0.5 Oe. The data also show that there is a rapid increase in ΔH_{eff} as one enters the manifold region. The increases shown, as well as the apparent structure in the manifold region, are accompanied by very large degradations in the cavity Q , from about 22 000 down to below 5000. Since the effective linewidth measurement is based on a small perturbation of the cavity Q , the high losses in the manifold region cannot be taken as

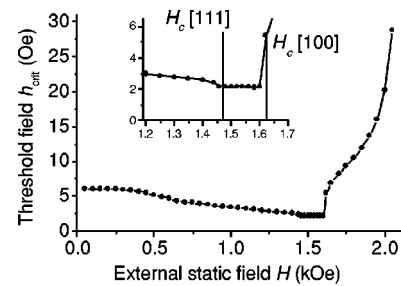


FIG. 4. Spin wave instability threshold microwave field amplitude h_{crit} as a function of the static external field H for parallel pumping at 9.0 GHz for the hipped yttrium iron garnet 2.04 mm diam sphere. The inset shows a detailed view of the flat minimum h_{crit} region. The vertical lines in the inset indicate calculated static field H_c values for which h_{crit} would be minimum for independent grains with [111] or [100] crystallographic axes parallel to \mathbf{H} , as indicated.

accurate measures of the actual losses. Accurate measurements of the in-manifold effective linewidth are in progress.

The data in Fig. 3 are typical of the effective linewidth versus field response which is found for dense polycrystalline ferrites.^{8,21} (1) Both the high-field and low-field ΔH_{eff} values are quite small compared to the FMR linewidth. The high-field ΔH_{eff} of 1.7 ± 0.5 Oe compares to the results for dense polycrystalline ultra pure YIG.¹⁰ (2) The slightly larger ΔH_{eff} for fields below the manifold region is attributed to residual two-magnon scattering to high- k spin waves. (3) The rapid increase in ΔH_{eff} as one approaches the manifold region from either side is due to the onset of two-magnon scattering to low- k modes. Patton has shown that the effective linewidth in the manifold region can be accurately modeled in terms of the TMAS process,⁸ based on the effective linewidth analysis of Schlömann.²²

V. BUTTERFLY CURVES AND SPIN WAVE LINEWIDTH

As outlined in Sec. III, detailed measurements of the spin wave instability threshold h_{crit} versus the static external field H were obtained for the sphere and disk samples at 9 and 16.7 GHz. This section will focus on the data and analysis for the 2.04 mm diam sphere. The other samples and other geometries gave similar results.

A. Parallel pumping butterfly curve data

Figures 4 and 5 show the results of the high-power parallel pumping measurements for the 2.04 mm diam sphere sample at 9 and 16.7 GHz, respectively. The main graphs show the full h_{crit} versus H butterfly curve responses from zero field up to the high-field limit for half-frequency spin waves. The insets show the low-threshold data at the so-called bottom of the butterfly curve on an expanded scale. The vertical lines in the insets indicate calculated static field values for which h_{crit} would be minimum for independent single crystal grains with [111] or [100] crystallographic axes parallel to \mathbf{H} . The static field points for the lower and upper field boundaries are labeled as $H_c[111]$ and $H_c[100]$, respectively.

While the overall butterfly curve profiles are typical of those found in dense polycrystals, the inset data represent a different effect. First consider the expected features.

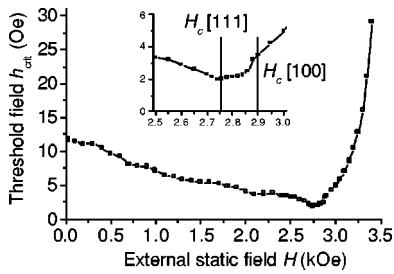


FIG. 5. Spin wave instability threshold microwave field amplitude h_{crit} as a function of the static external field H for parallel pumping at 16.7 GHz for the hipped yttrium iron garnet 2.04 mm diam sphere. The inset shows a detailed view of the minimum h_{crit} region. The vertical lines in the inset indicate calculated static field H_c values for which h_{crit} would be minimum for independent grains with [111] or [100] crystallographic axes parallel to \mathbf{H} , as indicated.

- (1) The measured h_{crit} values are relatively small. The minimum threshold values of 2 Oe or so for the 9 GHz data, for example, give spin wave linewidth ΔH_k values of about 1 Oe. These values are of the same order as found in hot pressed dense polycrystalline YIG¹⁰ and are larger than in single crystals.²³ Note that the minimum h_{crit} value at 16.7 GHz is about the same as at 9 GHz. This implies a lower spin wave linewidth at 16.7 GHz than at 9 GHz. This comparison will be an important consideration in the next section.
- (2) These minimum threshold values occur for H values close to 1.5 kOe for pumping at 9 GHz and 2.75 kOe for pumping at 16.7 GHz. These minimum threshold field regions correspond to the point where the wave number k values for the critical modes are close to zero. These $k \approx 0$ modes actually have wave numbers on the order of 10^4 rad/cm.
- (3) As one moves down in a static field from the minimum h_{crit} regions in (2), the increase in h_{crit} corresponds to an increase in the critical mode wave number and a spin wave linewidth ΔH_k which increases with k . The ΔH_k versus k analysis and interpretation is considered below.
- (4) Finally, the small but distinct change in the h_{crit} versus H response as the field drops below the saturation field limit at $H_s \approx 0.6$ kOe indicates the onset of demagnetizing effects as the sphere drops below magnetic saturation. The fields at which these changes occur are consistent with the hysteresis data in Fig. 1 and the sphere saturation fields noted in Table I.

As noted above, the unexpected features in the h_{crit} versus H responses shown in Figs. 4 and 5 are in the distinct regions close to the bottom of the butterfly curves. As shown in the Fig. 4 inset, the 9 GHz data give a perfectly flat h_{crit} versus H response for fields between the indicated $H_c[111]$ and $H_c[100]$ field limits. The 16.7 GHz data show a similar effect, except that the linear h_{crit} versus H response between these two field limits has a small tilt. The $H_c[111]$ and $H_c[100]$ field boundaries represent the theoretical points in static external field for the parallel pump minimum threshold for single crystal spheres with the field oriented in these directions. The corresponding external static fields for a minimum h_{crit} for other orientations fall between these two limits.

The flat h_{crit} versus H response between $H_c[111]$ and $H_c[100]$, as at 9 GHz, or with a small tilt, as at 16.7 GHz, is an indication that the nonlinear spin wave instability processes occur *independently* within individual grains. There are a large number of grains and the random angular distribution leads to the uniform responses shown in the Fig. 4 and Fig. 5 insets. The almost perfect matching of the linear or tilted response interval with the $H_c[111]$ and $H_c[100]$ fields makes a clear and quantitative connection with the magnetocrystalline anisotropy in the hipped polycrystal.

B. Spin wave linewidth analysis

The high-power data in Figs. 4 and 5 for fields below the $H_c[111]$ boundary were further analyzed in order to make quantitative determinations of the spin wave linewidth as a function of wave number. The analysis was based on the standard Schlömann theory of parallel pumping in saturated isotropic ferrites.^{9,22} This theory gives the spin wave instability threshold h_c for a given mode at a frequency ω_k equal to one-half the pump frequency ω and with a wave vector \mathbf{k} as

$$h_c = \frac{\omega}{|\gamma|4\pi M_s} \frac{\Delta H_k(\omega, \mathbf{k})}{\sin^2 \theta_k}, \quad (3)$$

where θ_k is the angle between \mathbf{k} and the static field \mathbf{H} . As discussed in Sec. III, the spin wave linewidth parameter ΔH_k is related to the relaxation rate of the corresponding spin wave mode. This ΔH_k can be, and usually is, a function of the frequency and the wave vector \mathbf{k} .

The observed threshold h_{crit} will correspond to the minimum possible value of h_c over all available modes at $\omega_k = \omega/2$. The spin wave mode k and θ_k values at this minimum threshold point define the critical mode. These values are determined from the applicable spin wave dispersion relation

$$\omega_k = |\gamma| \sqrt{(H_i + Dk^2)(H_i + Dk^2 + 4\pi M_s \sin^2 \theta_k)}, \quad (4)$$

where H_i denotes the internal static field and D is an exchange stiffness parameter. For the sphere geometry of interest and isotropic material, one has $H_i = H - 4\pi M_s/3$. For cubic anisotropy and H along the [111] axis, one has $H_i = H - 4\pi M_s/3 - 4H_A/3$. For H along the [100] axis, one has $H_i = H - 4\pi M_s/3 + 2H_A$. For YIG materials, D is equal to 5.19×10^{-9} Oe cm²/rad.^{3,23}

The minimum threshold regions between $H_c[111]$ and $H_c[100]$ in Figs. 4 and 5 correspond to an $H = H_c$ point in the isotropic theory at which the minimum threshold critical modes have $k=0$ and $\theta_k = \pi/2$. As one moves below $H = H_c$, the minimum threshold critical modes have $\theta_k = \pi/2$ and $k = [(H_c - H)/D]^{1/2}$. The actual shape of the computed butterfly curve will depend on the frequency and \mathbf{k} dependence of ΔH_k . In general, one does not know, *a priori*, either the frequency or the wave vector dependencies of ΔH_k . Because of this problem, an empirical approach is usually adopted. In this approach, measured values of h_{crit} versus H are used in combination with the theory to extract empirical frequency and \mathbf{k} dependences for ΔH_k .⁹ This approach will be followed here.

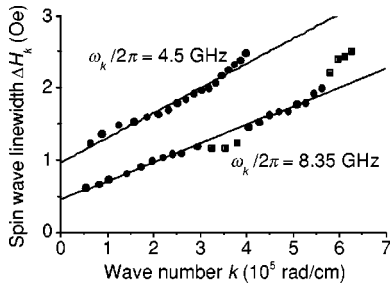


FIG. 6. Spin wave linewidth ΔH_k as a function of spin wave critical mode wave number k , based on the threshold data in Figs. 4 and 5. The solid circles and squares show the ΔH_k values extracted from the data. The solid lines show linear fits to the solid circle data points. The applicable spin wave frequencies are indicated and are equal to one-half of the corresponding pumping frequencies in Figs. 4 and 5.

Figure 6 shows the result of such an analysis, based on the data of Figs. 4 and 5, and with the $H_c[111]$ boundaries indicated in the figure insets taken as the $k=0$ cutoff field H_c . Only data for H above the 600 Oe limit for magnetic saturation were used for the ΔH_k determinations. The graph shows the spin wave linewidth ΔH_k as a function of the critical mode wave number k as extracted from the data. The solid circles and squares show the empirical ΔH_k values so obtained. The data shown by the squares are broken out to demonstrate special effects which are considered below. The lines show linear fits to the solid circle points. The applicable spin wave frequency is indicated for each set of results. Keep in mind that the indicated spin wave critical mode frequencies of 4.5 and 8.35 GHz correspond to one-half of the actual pump frequencies of 9 and 16.7 GHz, respectively, in Figs. 4 and 5.

The 8.35 GHz solid square data points in Fig. 6 show two effects that push the empirical ΔH_k values off the linear response defined by the circle data points. First, the departure from the linear fit for k values above about 5.8×10^5 rad/cm is related to the onset of intrinsic three-magnon splitting processes.²³ For parallel pumping at 8.35 GHz, such processes are allowed for k values above about 6×10^5 rad/cm. This increase is *not* due to sample demagnetization. Second, the apparent dip in ΔH_k centered at about $k \approx 3.5 \times 10^5$ rad/cm is attributed to some type of microstructure effect.

Apart from the effects shown by the solid square points in Fig. 6, the ΔH_k versus k results show that the response at both frequencies is approximately linear. If the indicated fits are taken to have the form $\Delta H_k = \Delta H_{k \rightarrow 0} + Bk$, the corresponding $\Delta H_{k \rightarrow 0}$ and B values are 0.97 Oe and 3.4×10^{-6} Oe cm/rad, respectively, for the critical mode spin waves at $\omega_k/2\pi = 4.5$ GHz and 0.45 Oe and 2.6×10^{-6} Oe cm/rad for the spin waves at $\omega_k/2\pi = 8.35$ GHz. The $\Delta H_{k \rightarrow 0}$ parameter is a measure of the relaxation rate for critical modes at $k \approx 0$, and the corresponding $\Delta H_{k \rightarrow 0}$ values may be compared with FMR and effective linewidths extrapolated to these same frequencies. The B parameter provides a measure of the increase in the spin wave linewidth with wave number at $\theta_k = \pi/2$.

The $\Delta H_{k \rightarrow 0}$ value of 0.45 Oe for 16.7 GHz pumping and $\omega_k/2\pi = 8.35$ GHz is the lowest $\Delta H_{k \rightarrow 0}$ ever reported for

polycrystalline YIG. Moreover, it is very close to the typical FMR linewidth value of 0.5 Oe at 9 GHz for single crystal YIG.³ The $\Delta H_{k \rightarrow 0}$ value of 0.97 Oe for 9 GHz pumping and $\omega_k/2\pi = 4.5$ GHz, when scaled up to $\omega_k/2\pi = 9$ GHz, will double to almost 2 Oe. When scaled to a common frequency, then, one can see that there is a *factor of 4* discrepancy between the $\Delta H_{k \rightarrow 0}$ values from the two sets of data. This discrepancy is suggestive of different mechanisms at the two frequencies.

Both of the above B values are about a factor of 5 larger than found for parallel pumping in YIG single crystals, where B is about 0.5×10^{-6} Oe cm/rad and approximately constant with frequency.^{23,24}

How can these spin wave linewidth results be explained? One possibility is related to microstructure-limited spin wave lifetimes. It has been established that the parallel pump ΔH_k scales with the inverse of the average grain size in polycrystalline ferrites.⁹ This type of response has been explained in terms of a transit time (TT) model.¹⁰ In this model, the spin waves are taken to have lifetimes that are limited by a microstructure-related scattering length. In Refs. 9 and 10, this scattering length was taken to scale with the grain size. The flat minimum threshold data in Figs. 4 and 5 indicate that the parallel pumping processes at low k in these hipped materials do indeed occur grain by grain.

One can make the TT analysis quantitative. From the dispersion relation of Eq. (4), critical modes with a nonzero k and $\theta_k = \pi/2$ will have a group velocity v_g given by

$$v_g = \frac{\partial \omega_k}{\partial k} = \frac{2|\gamma|^2 Dk}{\omega_k} (H_c - 4H_A/3 + 2\pi M_s/3). \quad (5)$$

The spin wave linewidth and the spin wave lifetime T_k are related through $\Delta H_k = 2/|\gamma|T_k$. The TT constraint is given by $L = v_g T_k$, where L is some scattering length related to the microstructure. The TT-limited spin wave linewidth is then given by

$$\Delta H_{kTT} = \left[\frac{4|\gamma|D(H_c - 4H_A/3 + 2\pi M_s/3)}{L\omega_k} \right] k. \quad (6)$$

One can see that the TT-limited spin wave linewidth is a linear function of k . If the TT model is indeed applicable here, the term in square brackets in Eq. (6) will correspond to the B value obtained experimentally. From the B values given above, the factor in square brackets in Eq. (6) gives L values of $\approx 70 \mu\text{m}$ for $\omega_k/2\pi = 4.5$ GHz and $80 \mu\text{m}$ for $\omega_k/2\pi = 8.35$ GHz. These values are in the same range and qualitatively consistent with a TT process.

While a TT process gives a spin wave linewidth which scales with the critical mode wave number and gives consistent scattering lengths for the two sets of data shown, it is noteworthy that the inferred scattering length is an order of magnitude larger than the average grain size of $8 \mu\text{m}$ for these hipped YIG materials. If a TT mechanism is indeed the origin of the measured B values, the further implication here is that the scattering lengths in these very dense polycrystalline YIG materials are *much greater* than the actual grain size. This means that the parametric spin waves are not always scattered at the grain boundaries. Based on the factor of

10 difference between L and the average grain size, one can set the probability of scattering at a given grain boundary at about 10%.

A reduced grain boundary scattering and an increased scattering length are consistent with the ultra dense nature of the hipped materials. Work by Scotter²⁵ indicates that the predominant scattering is related to the pores between the grains. All of the actual FMR linewidth data given above, moreover, point to an extremely small porosity.

From the above discussion, it appears that the observed k dependence of ΔH_k is consistent with a TT process. Of course, more work is needed to clarify the details of the scattering processes, the rather large scattering lengths, and definite connections with the microstructure. What about the $\Delta H_{k \rightarrow 0}$ values? As noted above, the $\Delta H_{k \rightarrow 0}$ value of 0.45 Oe for 16.7 GHz pumping is nearly identical with corresponding intrinsic linewidths in single crystals. On the other hand, the large $\Delta H_{k \rightarrow 0}$ for 9 GHz pumping and the factor of 4 increase after frequency scaling are inconsistent with the intrinsic process implicit in the higher-frequency data. There are, however, several nonintrinsic processes which can contribute to an increase in the relaxation rate at frequencies in the 3–5 GHz range. For YIG sphere samples, for example, the density of degenerate states goes through a maximum for ferromagnetic resonance at about 4 GHz.

Further work is needed to clarify and define these responses. One obvious problem is in the implication of single grain response from the flat butterfly curve minima in Figs. 4 and 5, juxtaposed with the large scattering lengths from the TT model. An important part of this work would be to determine v_g for low- k modes in particular sized single crystal grains. If the modes are constrained to individual grains, the spin wave dispersion may be different from that found for a large 2 mm diam spherical sample.

VI. SUMMARY AND CONCLUSION

The static magnetic and microwave properties of polycrystalline hipped YIG have been measured for disk and sphere samples. The measurements included (1) static magnetization, (2) half-power FMR linewidth ΔH_0 , (3) effective linewidth ΔH_{eff} , and (4) parallel pump spin wave linewidth ΔH_k . A reliable $4\pi M_s$ value of 1825 G was obtained for this material. This value is higher than generally accepted catalog values, but the 100% density of the material due to complete elimination of the porosity and high material purity make a value of $4\pi M_s = 1825 \pm 20$ G reasonable. The complete elimination of porosity was evident from the FMR linewidth data as well as direct density measurements.

The FMR linewidth measurements yielded an all time low ΔH_0 value of 13 Oe for pure polycrystalline YIG at the X band. This value agrees with calculated values of the two-magnon anisotropy scattering linewidth in large grain size YIG. The same theory also gives excellent quantitative agreement with the measured linewidths versus frequency from 9.5 to 18 GHz. The effective linewidth measurements at 10 GHz gave high-field values of 1.7 ± 0.5 Oe, slightly higher low-field values, and a characteristic increase in the

manifold region due to two-magnon processes. These data are consistent with previous results on dense coarse-grain YIG. The high-field ΔH_{eff} value of 1.7 Oe is about a factor of 3 larger than the corresponding intrinsic linewidth for single crystal YIG.

The parallel pumping data show, among other things, that the spin wave linewidth ΔH_k decreases in going from 9 GHz pumping to 16.7 GHz pumping. The data indicate a transit time effect and scattering lengths that are about a factor of 10 greater than the average grain size. For 16.7 GHz pumping, the extrapolated zero wave number spin wave linewidth of 0.45 Oe for critical mode spin waves at 8.35 GHz represents another all time low for a ΔH_k determination in polycrystalline YIG materials.

ACKNOWLEDGMENTS

This work was sponsored in part by the Office of Naval Research under Grants No. N00014-94-1-0096 and No. N00014-03-1-0070, the U.S. Army Research Office under Grant No. DAAG55-98-1-0430, the National Science Foundation under Grants No. DMR-9801649 and No. DMR-0108797, the Magnetic Materials Producers Association (A.V.N.), and the Natural Sciences and Engineering Research Council of Canada (D.M.). Richard G. Cox and Dr. Pieder Beeli are acknowledged for helpful discussions. R.G.C. is also acknowledged for assistance with the development of the microwave systems used for the measurements.

- ¹E. Schlömann, AIEEE Special Publication No. T-91, 1956 (unpublished), p. 600.
- ²E. Schlömann, *J. Phys. Chem. Solids* **6**, 242 (1958).
- ³M. Sparks, *Ferromagnetic Relaxation Theory* (McGraw-Hill, New York, 1964).
- ⁴K. Motizuki, M. Sparks, and P. E. Seiden, *Phys. Rev.* **140**, A972 (1965).
- ⁵P. E. Seiden and J. G. Grunberg, *J. Appl. Phys.* **34**, 1696 (1963).
- ⁶P. Röschmann, *IEEE Trans. Magn.* **14**, 1247 (1975).
- ⁷T. S. Kasatkina, Yu. M. Yakovlev, S. L. Matskevich, and I. K. Berestovaya, *Sov. Phys. Solid State* **25**, 999 (1983).
- ⁸C. E. Patton, *Phys. Rev.* **179**, 352 (1969).
- ⁹C. E. Patton, in *Magnetic Oxides*, edited by D. J. Craik (Wiley, London, 1975), Chap. 10, pp. 575–645.
- ¹⁰C. E. Patton, *J. Appl. Phys.* **41**, 1637 (1970).
- ¹¹H. J. Van Hook and C. B. Willingham, *Adv. Ceram.* **15**, 1637 (1984).
- ¹²H. V. Atkinson and S. Davies, *Metall. Mater. Trans. A* **31A**, 2981 (2000).
- ¹³G. Winkler, *Magnetic Garnets* (Vieweg & Sohn, Braunschweig, 1981).
- ¹⁴T. Inui and N. Ogasawara, *J. Appl. Phys.* **49**, 2019 (1978).
- ¹⁵J. J. Green and T. Kohane, *SCP Solid State Technol.* **7**, 46 (1964).
- ¹⁶J. R. Truedson, P. Kabos, K. D. McKinstry, and C. E. Patton, *J. Appl. Phys.* **76**, 432 (1994).
- ¹⁷A. V. Nazarov, C. E. Patton, R. G. Cox, L. Chen, and P. Kabos, *J. Magn. Mater.* **248**, 164 (2002).
- ¹⁸A. V. Nazarov, R. G. Cox, and C. E. Patton, *J. Appl. Phys.* **92**, 3890 (2002).
- ¹⁹A. V. Nazarov, Ph.D. thesis, Department of Physics, Colorado State University, 2002.
- ²⁰E. Schlömann, J. J. Green, and U. Milano, *J. Appl. Phys.* **31**, 386S (1960).
- ²¹Q. H. F. Vrehan, A. B. van Groenou, and J. G. M. de Lau, *Phys. Rev. B* **1**, 2332 (1970).
- ²²E. Schlömann, *Phys. Rev.* **182**, 632 (1969).
- ²³A. G. Gurevich and G. A. Melkov, *Magnetization Oscillations and Waves* (CRC Press, Boca Raton, 1996).
- ²⁴Yu. M. Yakovlev, Yu. N. Burdin, Yu. R. Shil'nikov, and T. N. Bushueva, *Sov. Phys. Solid State* **12**, 2475 (1971).
- ²⁵D. G. Scotter, *J. Appl. Phys.* **42**, 4088 (1971).